Asteroid Space Weathering and Regolith Evolution

Beth Ellen Clark
Cornell University

Bruce Hapke
University of Pittsburgh

Carlé Pieters
Brown University

Daniel Britt
University of Tennessee

Over time, exposure of airless bodies to the space environment results in optical changes to their surfaces. These optical changes are functions of the porosity, grain size distribution, and composition of the surface, and they depend on the relative rates of surface modification processes. Collectively, surface modification processes (such as impacts, solar wind ion implantation, sputtering, and micrometeorite bombardment) and their resulting optical effects have come to be known as "space weathering." Studies of lunar rocks and soils are the most important foundation we have on which to build an understanding of space weathering on asteroids. We cannot directly measure asteroid surfaces in a laboratory environment; therefore, we describe the lunar case, and compare it with the evidence for asteroids. In this chapter we review the evidence for space weathering on asteroids, including spectroscopy of optical effects, microscopy of physical effects, simulations of processes, lunar soils, meteorite breccias, spacecraft observations, and theoretical modeling. An understanding of space weathering is important to all remote-sensing studies of asteroid surfaces.

1. INTRODUCTION

We use the term space weathering to mean any surface modification process (or processes) that may tend to change the apparent traits (optical properties, physical structure, or chemical or mineralogical properties) of the immediate, remotely sensed surface of an airless body from analogous traits of the body's inherent bulk material. Studies of lunar soils and rocks brought back by the Apollo astronauts have provided important constraints on space weathering on the Moon (*Pieters et al.,* 2000; *Hapke,* 2001). These constraints have been used to account for the effects of space weathering in order to reveal underlying geologic/mineralogic patterns (*Lucey et al.,* 1995, 2000). However, space weathering effects on asteroids are not well understood because we do not have soils taken directly from the surface of an asteroid. We must therefore utilize indirect means to study space weathering on these bodies. A variety of evidence suggests that asteroid surfaces are characterized by complex particle size distributions (*Hörz and Cintala,* 1997), impact shock effects (*Keil et al.,* 1992), and mineral specific responses to impacts, solar wind, and cosmic-ray bombardment (*Sasaki et al.,* 2001; *Moroz et al.,* 1996; *Clark and Johnson*, 1996).

There is a variety of evidence that asteroids, except for the smallest ones, possess regoliths (of unknown depth). Asteroid regoliths were thought to be dominated by grains of a coarser average size than lunar regolith because asteroids are smaller (have weaker gravitational fields) and probably retain less impact ejecta (*Housen and Wilkening,* 1982; *Dollfus et al.,* 1989). Also, impact velocities are probably lower, so agglutination is less effective (*McKay et al.,* 1989). Polarization studies indicate surface grain sizes in the range of 30–300 μm (*Dollfus et al.,* 1989). Observations of 951 Gaspra and 243 Ida by the *Galileo* spacecraft revealed surfaces with degraded crater morphology and evidence of retained crater ejecta, suggesting that regolith formation and evolution processes were at work (*Sullivan et al.,* 1996; *Lee et al.,* 1996; *Carr et al.,* 1994; *Geissler et al.,* 1996). In addition, *NEAR Shoemaker* images of 433 Eros reveal infilled craters, distributed boulders, and abundant slump features. Taken together, these are strong evidence for a substantial regolith layer (*Veverka et al.,* 2001).

In this chapter we review the literature for constraints on asteroid space weathering. We discuss spectroscopic studies of optical effects, microscopic studies of physical effects, laboratory simulations of processes, lunar and meteorite evidence, pertinent spacecraft observations of asteroid surfaces, and theoretical modeling. This topic is important to asteroid researchers because space weathering affects the interpretation of all spectroscopic (compositional) observations of asteroids.

2. CHANGING PERSPECTIVE

One of the first to suggest that the space environment darkens material exposed on the lunar surface was *Gold* (1955). His prediction was amply confirmed when the Apollo samples of regolith were found to be darker, with redder continuum spectra, and more subdued absorption bands than pulverized lunar rocks of similar composition. It was postulated, based on experiments in which lunar rocks were vitrified in a N atmosphere, that the darkening was caused by impact-melted glass in the regolith. By an unfortunate quirk of nature, ferric impurities in glasses melted in N mimicked the spectral effects of space weathering and seemed to provide a ready explanation for them. Consequently, the idea that space weathering is caused by impact vitrification rapidly became widely accepted in the planetary science community, in spite of the evidence that vacuum-melted glasses are not dark. A suggestion by *Hapke et al.* (1975) that the spectral effects are due to vapor condensates was ignored, largely because there seemed to be no evidence for them in the lunar samples.

One of the first asteroids to be measured spectroscopically was Vesta, whose spectrum turned out to be strongly similar to those of particulate basaltic achondrites (*Bobrovnikoff,* 1929; *McCord et al.,* 1970). This seemed to provide a direct link between a group of meteorites and a probable parent body, and gave rise to the hope that other groups of meteorites and asteroids could be similarly linked. The strong resemblance between the spectra of Vesta and the achondrites also implied that space weathering did not operate in the asteroid belt. This was consistent with the paradigm that the optical changes were caused by agglutinate formation, because the velocities with which micrometeorites hit the surfaces of asteroids are generally thought to be too low for appreciable melting to occur (*Chapman and Salisbury,* 1973; *Matson et al.,* 1977; *McKay et al.,* 1989).

However, as time went on, the attempt to connect groups of asteroids and meteorites spectrally met with only limited success. In particular, no clear parent bodies were found for the most abundant class of meteorites, the ordinary chondrites, and no class of meteorites could be matched with one of the largest groups of asteroids, the S-class asteroids. Thus, the question arose as to whether the S asteroids might, in fact, be bodies of the same composition as ordinary chondrites, but with surfaces that have been altered by some kind of space weathering, either the same or different from the process that operates on the lunar surface. This gave rise to considerable discussion and sometimes heated debate (cf. *Matson et al.,* 1977; *Chapman,* 1995, 1996; *Bell,* 1995a,b, 1997, 1998; *Britt et al.,* 1992).

Meanwhile, optical, magnetic, electron spin resonance, and X-ray photoelectron spectroscopic evidence that reduced Fe is present in abundance on or near the surfaces of most lunar regolith particles continued to accumulate (see *Hapke,* 2001, and *Taylor et al.,* 2001a, for detailed descriptions). In addition, *Pieters et al.* (1993) showed that the spectral effects of lunar space weathering are concentrated in the smaller regolith particles (rather than agglutinates), and that the optical effects are caused by a surface, rather than a volume, phenomenon. Finally, Keller and his associates (*Keller and McKay,* 1993, 1997; *Keller et al.,* 1998, 1999; *Pieters et al.,* 2000), using improved transmission electron technology, documented that the regolith particles of a mature lunar soil are almost universally covered with thin, vapor-deposited coatings that contain abundant grains of submicroscopic metallic Fe, as predicted by the vapor deposition hypothesis.

There is no generally accepted term for the fine-grained Fe particles in the surface coatings. *Pieters et al.* (2000) used nanophase reduced Fe, $npFe^0$, which emphasized the scale of particles produced and their reduced nature. However, a significant amount of the optically active Fe in lunar soil is not nanometer-sized, but is in the >100-nm size range (*Hapke,* 2001). In addition, for at least 25 years the more general term "submicroscopic metallic iron" (SMFe) has been used (*Hapke et al.,* 1975).

Vapor condensates can be generated by two processes: solar wind sputtering and micrometeorite impact vaporization. Because of the lower velocities of the impactors in the asteroid belt, the second process is probably less effective there. However, the first process must operate, although at a reduced rate. *Hapke* (2000, 2001) has shown that the addition of as little as 0.025% SMFe can alter the spectrum of a powdered ordinary chondrite so that it strongly resembles that of an S asteroid. This may be compared to the 0.5% Fe required to convert the spectrum of a pulverized lunar rock into a regolith spectrum. Hence, the relevant question no longer is whether or not space weathering occurs on asteroids, but rather why some bodies appear pristine, while others have spectra that are altered.

3. ASTEROID-METEORITE CONNECTION

Studies of the asteroid-meteorite compositional connection concentrate on the evidence from spectral reflectance properties of materials in the wavelength region of ~0.35–3.2 μm. In this range, particulate minerals at the surfaces of airless bodies impart absorption bands on reflected light spectra that are diagnostic of the surface composition. Common parametric measurements of spectral reflectance include the albedo (total amount of light reflected), the depth of absorption bands (relative to the continuum), and the slope of the continuum, generally measured as rise over run from 0.7 to 1.5 μm (e.g., *McCord et al.,* 1981; *Clark and Roush,* 1984; *Pieters,* 1986). Telescopic and laboratory spectral work over the last 30 years (cf. *McCord et al.,* 1970; *Chapman and Salisbury,* 1973; *Gaffey et al.,* 1993; *Pieters and McFadden,* 1994) have established links between many asteroid spectral types and meteorite groups. Statistically, however, asteroid and meteorite spectra show consistent offsets in spectral parameters, possibly as a result of optical differences between bulk meteorites measured in the laboratory and asteroid surfaces measured remotely. For example, *Britt et al.* (1992) and *Burbine* (1991) have com-

TABLE 1. Space weathering and asteroid types.

Asteroid Type	Meteorite Analogs	Mineralogy	Alteration Effects
S	H, L, LL chondrites; stony irons, IAB irons, lodranites; winonites, siderophiles, ureilites	Olivine, pyroxene, metal	Albedo: up to 50% decrease Red slope: weak to moderate increase Band suppression: 50% decrease
V	Basaltic achondrites	Pyroxene, feldspar	Band suppression: 20%
A	Brachinites, pallasites	Olivine	Red slope: moderate increase Band suppression: 20% decrease?
Q	H, L, LL chondrites	Olivine, pyroxene, metal	Albedo: 20–30% decrease Band suppression: 20–30% decrease
Lunar	Lunar meteorites	Basalt, feldspar	Albedo: 50–75% decrease Red slope: moderate to strong increase Band suppression: 50–75% decrease

pared spectral parameters for asteroid and meteorite surveys and found significant mismatches even in the linked populations. Although space weathering may occur on all asteroids, many types lack the high albedo and strong spectral band contrasts that make weathering effects easily detectable. Asteroid types for which there is additional evidence of space weathering relative to their meteorite analogs include the S, V, A, and Q types. Shown in Table 1 are the probable meteorite analogs, estimated mineralogy, and inferred weathering effects. Note that the range in continuum slope change is 20–40% on average, although some lunar samples show strong increases of up to 300%. To illustrate weathering-related spectral alteration, Fig. 1 shows two examples of asteroid spectra with their likely meteorite analogs.

The Q asteroids, which have ordinary chondrites as their direct meteorite analog, show evidence of band suppression and albedo reduction. The olivine-rich A class shows a red continuum slope and modest band suppression consistent with weathering of olivine (*Sasaki et al.,* 2001). Within the V class, the largest V asteroid, 4 Vesta, shows subdued absorption features relative to many of the much smaller "vestoids" as well as the V-type meteorite analog, the basaltic achondrite meteorites (*Binzel and Xu,* 1993; *Hiroi et al.,* 1994, 1995). This suggests that some physical process or minor weathering has occurred on Vesta's surface, although Vesta may have been resurfaced by a major impact in its recent past (*Binzel and Xu,* 1993; *Pieters and Binzel,* 1994; *Hiroi et al.,* 2000). Figure 1 compares Vesta with a eucrite meteorite, thought to be an excellent match (*McCord et al.,* 1970). While the band centers and shapes are similar, Vesta shows a reduction in band depth indicative of space weathering. The strongest evidence for space weathering is for the S-type asteroids and the ordinary chondrites (OCs). The spectral band center data show that OCs have similar mineralogy to the S asteroids, but weathering processes appear to produce differences in band depth, red slope, and albedo.

Although the spectral data indicate that space weathering might occur on asteroids, some of the spectral trends are difficult to interpret and differ from lunarlike space weathering. Within the S-type asteroids there is a trend toward reduced 1.0-μm band depth with increasing diameter shown in Fig. 2 (*Gaffey et al.,* 1993). If larger-diameter asteroids have longer lifetimes and therefore older surfaces, this indicates an attenuation of band depth with increasing surface age.

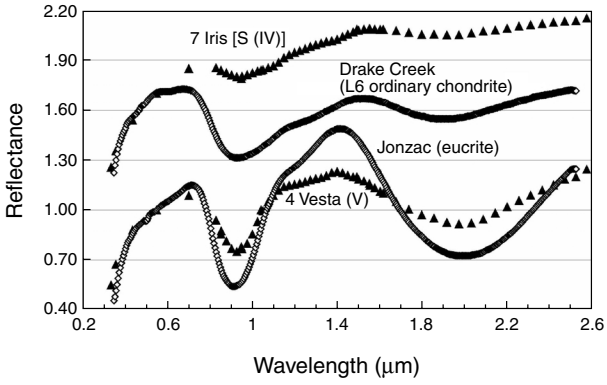

Fig. 1. Two examples of reflectance spectra of asteroids paired with their meteorite analogs. One plausible explanation for the spectral mismatches is that space weathering processes affect the surfaces of the asteroids, altering them from their original spectral properties. Asteroids are displayed as closed triangles and meteorites as open diamonds. The top pair is offset vertically by 0.7 for clarity and show the S (IV) asteroid 7 Iris with the L6 ordinary chondrite Drake Creek. Although both objects have approximately the same mineralogy as shown by their band minima, the spectra of 7 Iris is reddened by 30% relative to Drake Creek. Also, Iris's major absorption bands are significantly reduced. The pair of 4 Vesta and the eucrite Jonzac also show similar mineralogy, but the band depth of 4 Vesta is reduced by 40% relative to its analog meteorite.

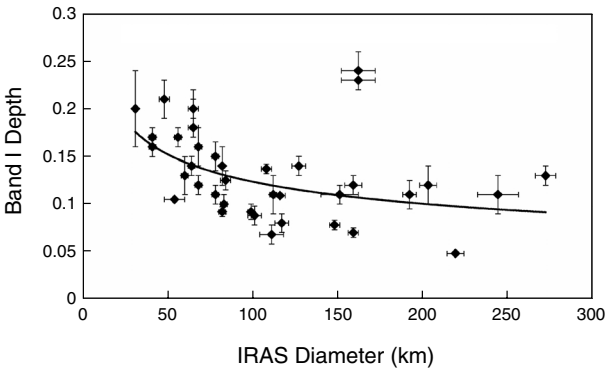

Fig. 2. For the population of S-type asteroids the depth of the 1.0-μm band (from *Gaffey et al.,* 1993) is plotted against estimated diameter (from *Tedesco et al.,* 1989). The trend toward shallower 1.0-μm bands with increasing size could show the effects of weathering increasing with surface age.

This tracks well with the idea that weathering reduces band depth over time. However, the other two spectral components of this process from the lunar case, albedo and spectral slope, tell a different story. There is essentially no trend with size for either slope or albedo in the S-type asteroids.

This lack of correlation may be explained by two factors. First, diameter is probably a fair proxy for surface age; however, for weathering purposes, what is critical is the age of the last global resurfacing event, which is unknown for any asteroid and probably random for this population. Numerical simulations indicate that gravitational retention of ejecta is less important on asteroids several kilometers in diameter, and these are not represented in Fig. 2. Second, the S-type asteroids are represented by a wide range of mineralogies that vary from almost pure olivine to almost exclusively pyroxene with wide ranges of mixtures between these extremes. Differing mineral chemistry probably responds differently to space weathering. However, restricting the analysis to mineralogically similar subgroups does not clear up this problem. For example, within the OC-like S(IV) subclass there is a strong trend toward reduced spectral slope with increasing asteroid size, which suggests that red slope is anticorrelated with surface age proxy in this critical subclass (*Gaffey et al.,* 1993). Also, for this subclass, increasing band depth is correlated with increasing red slope, which is the opposite of what would be expected with lunarlike weathering. On the other hand, there is a weak trend within the S(IV)s of reduced albedo with increasing red slope that follows the lunar trends.

Another line of evidence comes from telescopic observations of small (<20-km-diameter) S- and Q-type asteroids (*Binzel et al.,* 1996). In this distribution the 1-μm band depth forms a continuum between the relatively shallow band depths for S types to the relatively deep and therefore fresh Q types. The implication is that we are seeing a weathering continuum between fresh and weathered objects that corresponds to the surface age of the asteroid. This is probably true, but there is no way to determine surface age short of a sample return. These seemingly contradictory trends suggest that space weathering is occurring on S-type asteroids, but the details and the weathering products are different from the lunar case. It is perhaps not surprising that different mineralogies and different energy inputs produce different results.

4. SPACE WEATHERING: THE LUNAR EXAMPLE

Studies of the Moon have provided excellent materials for laboratory investigation of the physical and optical effects of lunar space weathering processes. Important reviews are available in *Hapke* (2001) and *Pieters et al.* (2000). In this section we briefly summarize our present knowledge, and we conclude with a description of the current model for lunarlike space weathering.

4.1. Surface Modification Processes

Processes known to affect the surface of the Moon include, but are not limited to, interplanetary dust and micrometeorite bombardment; electromagnetic radiation; solar wind ion implantation and sputtering; cosmic-ray bombardment; and meteoroid, asteroid, and comet impacts. One important result of these processes is the formation of reduced SMFe particles on grain surfaces, and this SMFe seems to dominate the optical effects. The SMFe also causes a characteristic electron spin resonance signal whose strength is denoted by I_s. A measure of the abundance of SMFe normalized to the abundance of FeO (I_s/FeO) is used as a good indicator of cumulative surface exposure, with "mature" soils having values greater than 60 (*Morris,* 1976, 1977, 1978, 1980).

4.2. Effects Observed with Lunar Samples

The physical effects of space-weathering processes on lunar soils have been studied carefully in the laboratory (e.g., *Heiken et al.,* 1991, Chapter 7). For example, particle size distributions of Apollo 17 lunar soils are shown in Fig. 3. Individual soils do not exhibit a history of continuous exposure, but can be described as a random product of reworking by micrometeorites and mixing with other soils. With time, finer particles are often combined by agglutination into larger particles. A mature soil reaches a "steady state" in which the process of pulverization is countered by agglutination and replenishment of coarser particles (*McKay et al.,* 1974). The mass fraction of particles <25 μm is typically on the order of 25% or less.

On the Moon, the optical effects of weathering in the space environment accumulate over time such that fresh subsurface materials "mature" at the surface. With exposure to the space environment, lunar soils generally darken and diagnostic absorption bands weaken. A mature lunar soil has a characteristic red-sloped continuum (reflectance increas-

ing toward longer wavelengths). Representative bidirectional reflectance spectra of several Apollo 16 lunar samples (I = 30°, e = 30°) are shown in Fig. 4. Most Apollo 16 rocks are feldspathic breccias and contain small amounts of low-Ca pyroxene. Because of their high plagioclase content, some can be quite bright. The mature soils of the region, however, are all relatively uniform: significantly darker especially at shorter wavelengths and with very little spectral contrast. Regolith breccias are typically darker than other more "pristine" rocks, but only rarely exhibit properties comparable to natural lunar soils.

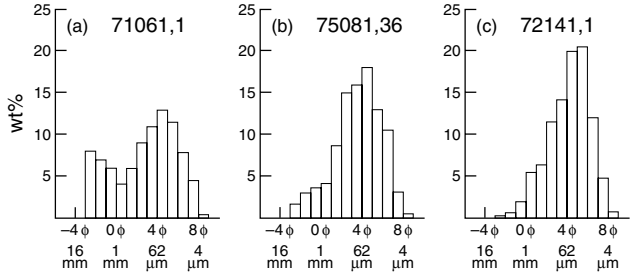

Fig. 3. Distribution of particle sizes in three Apollo 17 lunar soils in terms of mass (or volume %) of each size fraction (after *McKay et al.,* 1974): **(a)** An immature soil with a bimodal population of coarse and fine grains. **(b)** A submature soil. **(c)** A mature well-developed soil. The volumetric mean grain size of most well-developed lunar soils range from 45 to 75 μm.

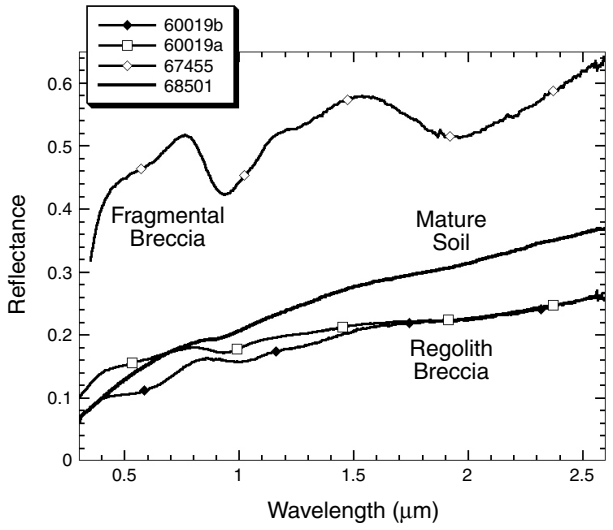

Fig. 4. Bidirectional reflectance spectra of typical Apollo 16 lunar samples (I = 30°, e = 0°). Mature soils such as 68501 have relatively weak features and exhibit a distinctive continuum with reflectance increasing toward longer wavelengths. Spectra for two different parts of regolith breccia 60019 are shown. These spectra from the same rock are quite different, but neither sample is similar to mature regolith from the region. In contrast, a typical noritic breccia (67455) from the site is bright and exhibits prominent absorption bands from low-Ca pyroxene.

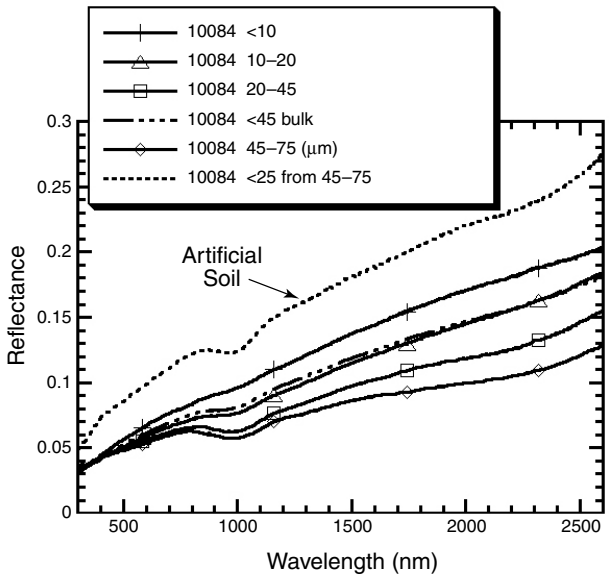

Fig. 5. Bidirectional reflectance spectra for size separates from a mature soil from Apollo 11 (10084) (data from *Taylor et al.,* 2001a; *Pieters et al.,* 1993). The bulk soil is indicated with a dot-dashed line and wet-sieved particle size separates are shown as solid lines. Note the bulk soil spectrum is dominated by the finest fractions rather than by the volumetrically dominant fractions. Note also that all size fractions of these natural soils converge at shorter wavelengths. An artificial fine fraction was prepared by grinding a subsample of the agglutinate-rich 45–75 fraction to <25 μm and is shown as a dotted line. The legend gives the size fraction in micrometers.

The initial study of the optical properties of lunar soils was carried out in the 1970s by several research groups (J. B. Adams, T. B. McCord, B. Hapke, and D. Nash). When laboratory facilities later became available to accurately measure the bidirectional reflectance properties of small (30 mg) subsamples of lunar soil, additional properties of lunar soils became apparent. Specifically, the finest fractions were shown to dominate the optical properties of bulk soils even though the greater mass is in the larger particles (*Pieters et al.,* 1993). Shown in Fig. 5 are spectra of the bulk soil and size separates for Apollo 11 mature soil 10084. Even though the more abundant (by weight) size fractions greater than 20 μm exhibit relatively strong absorption bands, the bulk soil is clearly most similar to the <20-μm fractions. Furthermore, the optical properties of natural lunar soils cannot be reproduced artificially. All size fractions are agglutinate rich, but when the 45–75-μm fraction was ground to <25 μm it is unnaturally bright at all wavelengths. The optical properties of this lunar artificial <25-μm soil separate are totally inconsistent with those of the natural <25-μm fraction. The anomalous properties of the manually ground soil sample was an important indication that the weathering products of natural lunar soils are surface correlated (*Pieters et al.,* 1993).

A detailed coordinated analysis of the compositional and optical properties of a suite of selected lunar soils has re-

cently been carried out for mare soils (*Taylor et al.,* 2001a) and is in progress for highland soils (*Taylor et al.,* 2001b). Several critical insights have come from this modern study: (1) A regular variation of composition with grain size is well documented and is dominated by concentration of feldspathic components in the finer fractions. (2) The amount of agglutinitic glass increases with decreasing grain size, as does the amount of nanophase-reduced Fe, but the nanophase Fe increases at a *much* greater rate. (3) The surfaces of individual grains were shown to contain compositions clearly foreign to the grain itself (Fe-rich rims on plagioclase; Al-rich rims on pyroxene), indicating mobility of atoms during exposure to the space environment. The latter two observations by this consortium are additional indications that the products of space weathering are surface correlated. These observations of where space-weathering products occur have now been beautifully documented with transmission electron microscopy (TEM) images of individual soil grains carried out by *Keller et al.* (1999) and *Pieters et al.* (2000). TEM images of anorthosite grains from a mature lunar soil shown in Fig. 6 exhibit abundant nanophase-reduced Fe on the rims. Since anorthosite is almost Fe-free, the origin of the observed SMFe must be from other sources. Such images document the surface deposition of nanophase Fe from solar wind sputtering and/or vapor fractionation that occurs during micrometeorite impacts. Both processes release atoms from one grain to be deposited on another.

Bidirectional reflectance spectra of the finest fraction (<10 μm) of lunar soils from the consortium study (*Noble et al.,* 2001) illustrate the optical effects of nanophase-reduced Fe accumulation on the surface of soil grains (Fig. 7). The finest fraction is well suited to document the effects of space weathering since the path length through these particles is small but the surface area/volume large. The optical effects of nanophase-reduced Fe are nonlinear (*Pieters et al.,* 2000; *Noble et al.,* 2001; *Hapke,* 2001): Small amounts redden the visible portion of the spectrum with little effect on longer wavelengths, whereas larger amounts dominate the spectrum, producing an almost linear continuum. This is readily seen in the spectra of Fig. 7. The highland soils have the least nanophase-reduced Fe and the mare soils the most, a direct result of the availability of Fe in the soil.

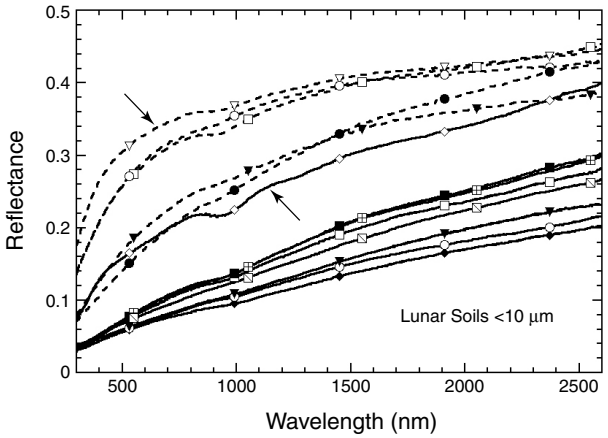

Fig. 7. Bidirectional reflectance spectra of the finest fraction (<10 μm) of lunar soils (after *Noble et al.,* 2001) illustrating the optical effects of SMFe accumulation on the surface of soil grains. Highland soils are indicated with dashed lines and mare soils with solid lines. The most immature soil of each (I_s/FeO < 15) is indicated with an arrow. The finest fraction is well suited to document the effects of space weathering since the path length through these particles is small but the surface area/volume is large. The highland soils have the least SMFe and the mare soils the most, a direct result from the availability of iron in the soil.

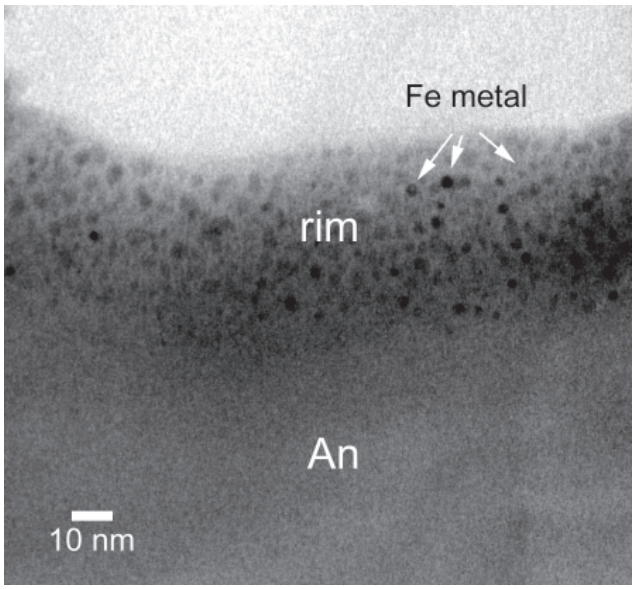

Fig. 6. TEM image of an anorthosite (An) grain from a mature lunar soil that exhibits a rim of Fe metal particles (SMFe) (from *Keller et al.,* 1999; *Pieters et al.,* 2000).

4.3. Lunar Model

It is important to realize that we have only the lunar studies to serve as a foundation on which to build a model for space weathering of the asteroids. Because we cannot directly describe asteroid space weathering, we instead describe the lunar case and compare it with the evidence for asteroids (*McKay et al.,* 1989). Currently the model for space weathering on the Moon that is most consistent with all the observations is that micrometeorite and solar wind bombardment produce a vapor from target particulate materials that, upon redeposition at the surface, is chemically reduced such that ferrous Fe previously existing in silicates condenses out as metallic Fe in submicroscopic spheres embedded in the mineral coatings on individual grains (*Hapke,* 2000). The formation and accumulation of the SMFe results in changes of the chemical, mineral, optical, and physical properties of the immediate surface and all subsequent

generation of products (agglutinates). Although this process probably dominates the optical maturation of the lunar regolith, it does not explain all the differences observed between mature and immature soils. In addition, the combination of the processes of agglutinate formation, particle shock and comminution, crystal damage due to cosmic rays, and SMFe deposition are probably important. Lunar surface alteration can take millions of years and is an ongoing process since major impacts excavate and distribute fresh material.

5. METEORITE EVIDENCE

Much of what we know about the geochemistry of asteroids comes from the "ground truth" provided by meteorites. Samples from several meteorite groups show evidence of surface exposure and carry at least some information on the effects of regolith processes. The "solar-wind-implanted gas-rich" meteorites contain grains that have low-energy solar wind particles implanted into their surfaces. For this implantation to occur, the grain had to be directly exposed to the solar wind and thus had to be on the surface of an atmosphereless body. The gas-rich meteorites are typically breccias that contain a mixture of fine-grained gas-rich regolith soil and larger rock fragments that have been fused together by grain-boundary melting. This mixture probably was once a loose regolith that was relithified by impact shock and heating. Gas-rich ordinary chondrites are characterized by a light-dark structure (*Heymann,* 1967) where the gas-rich fine grained material is much darker than the rock fragments. This structure is shown in Fig. 8 in the gas-rich H6 ordinary chondrite Dwaleni. Spectrally the gas-rich portions of these meteorites can be up to a factor of 2 darker than the adjacent rock fragments and the spectral absorption bands are similarly suppressed. This suggests that some of the effects of asteroidal regolith processes in OCs are to darken the surface material and suppress spectral bands. Similar effects are seen in the black OCs, which show darkening and band suppression from the effects of shock (*Britt and Pieters,* 1994). These meteorites are not solar-wind gas-rich, but probably are highly shocked material from the lower levels of large impact craters (*Keil et al.,* 1992).

Other meteorite groups that show evidence of regolith-related alteration include enstatite chondrites and eucrites. The enstatite chondrite Abee (E4) is brecciated and shock-blackened (*Rubin et al.,* 1997). Its reflectance is about a factor of 2 lower than other enstatite chondrites. The eucrite Juvinas has shock-blackened areas and shows reduced reflectance and moderately subdued absorption bands (*Gaffey,* 1976). Solar-wind-implanted gases are also found in many carbonaceous chondrites, particularly CI and CM chondrites (*Keil,* 1982). However, there are essentially no spectral differences between gas-rich and gas-poor carbonaceous chondrites. These meteorites may not show any optical effects from regolith action because the abundance of opaque oxides and carbon compounds that characterize these meteorites normally produce a low albedo and suppressed absorption features.

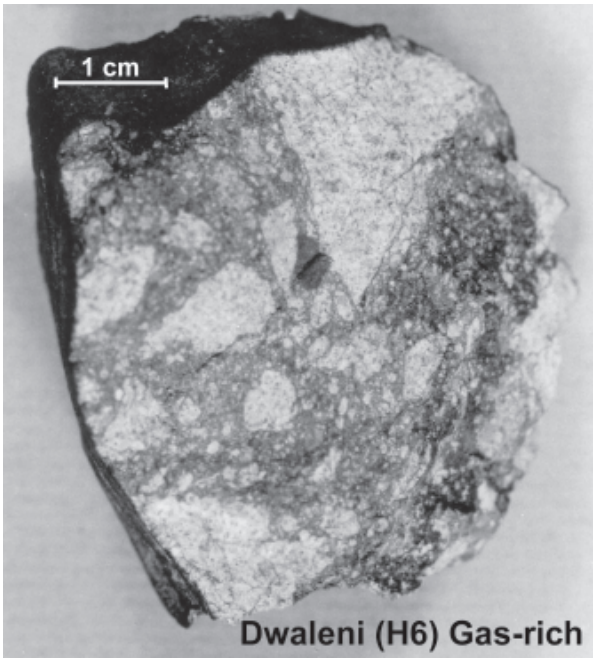

Fig. 8. The gas-rich ordinary chondrite Dwaleni (H6) shows the effects of exposure to the space environment. The dark, fine-grained material in this meteorite was probably once part of the regolith soil of its parent asteroid and preserves some of the darkening and spectral band reduction caused by space weathering.

Although gas-rich OCs show strong evidence of once being part of the surface layer of asteroids, and of darkening and band attenuation, there is no evidence of the characteristic red spectral slope of the S-type asteroids (*Britt and Pieters,* 1994). Shown in Fig. 9 is a plot of albedo vs. red slope for ordinary chondrites, S-type asteroids, and lunar soils. In lunar terms, all S-type asteroids are immature as shown in Fig. 9. This relative immaturity is probably the result of a combination of several factors: (1) The lower average impact velocities in the asteroid belt (~5 km/s vs. ~15 km/s on the Moon) produce much less melting, vaporization, and alteration. It may take much longer for an asteroidal surface to mature because of these lower energies, and because of the lower gravity. (2) The fundamental mineralogical differences between the feldspar normative Moon and the olivine normative S-type asteroids produce somewhat different alteration products during micrometeorite impact (*Keil,* 1982). (3) The much smaller sizes and lower gravity regimes of asteroids produce much more global distributions of fresh ejecta from major impacts. Although the range of red slopes in OCs slightly overlap the range in S-type asteroids, there is essentially no red slope in OCs and gas-rich OCs are no redder than other OCs.

Why aren't gas-rich ordinary chondrites spectrally red? There are several factors working against the preservation of a strong red slope signal in gas-rich OCs. First, the formation of meteorites strong enough to survive excavation, transport to Earth, atmospheric entry, and landing requires

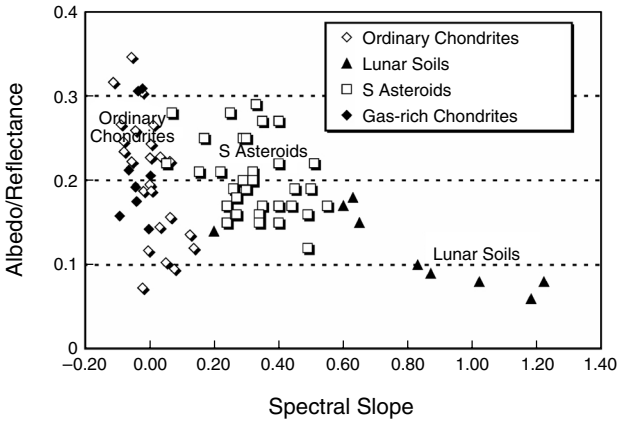

Fig. 9. The reflectance of ordinary chondrite meteorites, S-type asteroids, and lunar soils compared to their red continuum slope. The ordinary chondrites show essentially no red slope with slope increasing through the S-type asteroids to an extreme in the mature lunar soils. Note that increasing slope is correlated with decreasing reflectance. S-type asteroids are moderately red-sloped, but would be considered immature in lunar terms. Ordinary chondrites exhibit the full range of reflectance change, but show no increase in red slope.

the relithification of the regolith soil by grain-boundary melting. This kind of melting would strongly affect any SMFe metallic surface layers, which would remelt long before the silicates, and tend to form larger, less optically active particles. Second, gas-rich ordinary chondrites are intimate mixtures of surface and nonsurface materials (Fig. 2). Typically, the regolith-derived grains are much less than 50% of the volume of a gas-rich meteorite. Any red slope signal in these mixtures would be severely diluted by the stronger spectral signature of the fresh material. Finally, the red slope in S-type asteroids is fundamentally weaker than the lunar signal. It is easier to dilute the S-type red spectral slope than it is to affect the lunar red spectral slope because of the relative strengths of the signatures.

Fanale et al. (1992) compared S-type asteroid albedos and OC meteorite reflectances and showed that there was significant overlap in values, indicating a possible genetic relationship between the two populations. However, in that study Fanale et al. did not take into account the fact that OCs are measured at a viewing geometry that differs from that used for the calculation of asteroid albedos. Asteroid albedo values are measurements of the geometric albedo — defined as the ratio of the brightness of a body at 0° phase angle to the brightness of a perfect Lambert disk of the same radius and at the same distance as the body, but illuminated and observed perpendicularly (*Hapke,* 1993). Laboratory reflectance quantities are generally bidirectional reflectance factors, defined as the ratio of the brightness of a sample at 30° incidence and 0° emission, to the brightness of a Lambert surface illuminated identically (e.g., *Pieters,* 1983). At any given wavelength, the value of the geometric albedo (0° phase) is therefore systematically higher than the value of the bidirectional reflectance of a laboratory sample (30° phase). According to the photometric studies of *Shkuratov et al.* (1999) and *Clark et al.* (2002), the difference can be up to a factor of 2.5 due to significant opposition surge at 0° phase. Thus, taking viewing geometry into account, the results of *Fanale et al.* (1992) indicate that meteorites are actually up to 2.5× brighter than asteroids on average. In other words, S-type asteroids are generally much darker than OC meteorites. Thus, if OCs come from S types, this could be evidence that optical darkening (space weathering) occurs on asteroids.

6. LABORATORY SIMULATIONS

A large number of experiments have been carried out in the laboratory in attempts to simulate possible lunar or asteroidal space-weathering processes. These include the following: vitrification to simulate impact melting, ion irradiation to simulate solar wind bombardment, evaporation and subsequent condensation to simulate impact vaporization, and pulsed laser irradiation to simulate micrometeorite bombardment. These experiments are discussed briefly here, and they are described in detail and critically analyzed in *Hapke* (2001).

6.1. Vitrification

The lunar regolith contains abundant glass, mostly as part of agglutinate particles. In fact, some confusion exists in the literature because quench glass is often not distinguished from amorphous agglutinates. *Conel and Nash* (1970) and *Adams and McCord* (1971) melted lunar rocks in a nitrogen atmosphere and produced a material that had a low albedo and a reddened spectrum with subdued absorption bands. They initially proposed that lunar space weathering is due to simple impact vitrification. This was later modified to attribute the effects to accumulation of agglutinates. However, when *Hapke et al.* (1975) and *Wells and Hapke* (1977) melted lunar rocks in vacuum the resulting glass had a high albedo with a spectrum that was unreddened and had strong, broad absorption bands. A similar study by *Bell et al.* (1976) documented the effects of f_{O_2} and composition on the optical properties of quench glass. Quench glasses are quite different from agglutinitic glass and appear to have little effect on the properties of most lunar soils. *Hapke et al.* (1975) also suggested that the early N-melted quench glasses were oxidized and that their optical properties were caused by ferric Fe, which is not present in the lunar regolith. Similar objections apply to later vitrification experiments reported by *Clark et al.* (1992) and *Cloutis and Gaffey* (1993).

6.2. Ion Irradiation

Bombardment of silicate rock powders by H and He ions of kilovolt energies have been carried out by several groups, including Wehner and his colleagues (*Rosenberg and Wehner,* 1964; *KenKnight et al.,* 1967); *Hapke* (1966, 1968,

1973); and *Dukes et al.* (1999). Irradiation of a smooth surface has no effect on the optical properties. However, irradiation of a powder results in darkening, reddening, and decreased depth of absorption bands caused by the accumulation of absorbing sputter-deposited coatings on the grains. *Dukes et al.* (1999) showed that He^+ irradiation is more effective than H^+ in surface reduction of Fe in olivine.

6.3. Evaporation-Condensation

Hapke et al. (1975) and *Cassidy and Hapke* (1975) evaporated lunar and terrestrial silicates in an electron beam furnace and condensed some of the vapor onto fused silica microscope slides. The condensates had a transmission spectrum that decreased monotonically with increasing wavelength, with no discrete absorption bands. The vapor deposits were also found to exhibit the characteristic lunar ferromagnetic resonance and electron spin resonance exhibited by metallic Fe particles tens of nanometers in size (*Morris,* 1976). *Hapke et al.* (1975) showed that the condensation process is inherently reducing and results in the production of the Fe particles. They also showed that such particles can account for the optical properties of the coatings. They proposed that lunar space weathering was caused by coatings containing SMFe generated by both solar wind sputtering and impact vaporization in the lunar regolith.

6.4. Laser Shots

Hapke et al. (1975) irradiated a lunar glass with a pulsed laser. The resulting condensate was brownish. *Moroz et al.* (1996) and *Yamada et al.* (1999) bombarded silicate powders with laser pulses and found that the powders darkened and reddened. *Moroz et al.* (1996) interpreted their results as caused by melting; however, it is likely that the darkening is also due to condensates of the vapor generated by the laser shots. This was corroborated by the results of *Sasaki et al.* (2001), who used nanopulse laser shots to simulate space weathering, and found direct evidence for SMFe-bearing condensates on grain surfaces resulting from the laser evaporation and condensation. These experiments indicate that olivine is more easily weathered than pyroxene (*Yamada et al.,* 1999; *Hiroi and Sasaki*, 2002).

7. MODELING OPTICAL EFFECTS

The effects of the SMFe in the vapor condensates on the optical properties of a regolith can be modeled analytically using the reflectance spectroscopy formalism in *Hapke* (1993). The model is described in detail in *Hapke* (2001) and will only be summarized here.

The bidirectional reflectance of a medium of isotropically scattering particles can be described to a good approximation by

$$r(i, e, g) = (w/4\pi)[\cos i/(\cos i + \cos e)]H(w, i)H(w, e)$$

where w = single scattering albedo, i = angle of incidence, e = angle of emergence, $H(w, x) = (1 + 2x)/[1 + 2x(1 - w)^{1/2}]$.

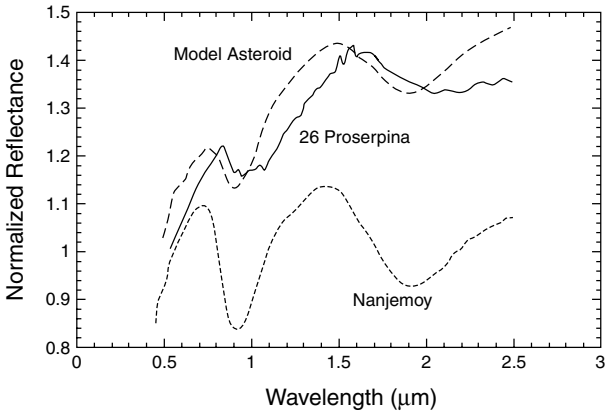

Fig. 10. Plot showing the effect of adding a 0.025% SMFe to a pulverized ordinary chondrite, Nanjemoy. In this example, n_h = 1.70, and the complex refractive index of Fe measured by *Johnson and Christy* (1974) was used. The resulting normalized spectrum is compared with that of a typical S asteroid, 26 Proserpina (shown offset for clarity). Lunar regolith typically contains about 0.5% SMFe. Thus, only about one-twentieth as much space weathering apparently occurs in the asteroid belt as on the lunar surface. Note that adding the Fe does not change the wavelengths of the band centers, only their depths.

The equivalent slab model expression for the single scattering albedo is

$$w = S_e + (1 - S_e)(1 - S_i)e^{-\alpha D}/(1 - S_i e^{-\alpha D})$$

where S_e = reflection coefficient for light incident on the particle surface from outside, S_i = reflection coefficient for light incident on the particle surface from inside, α = particle absorption coefficient, and D = mean particle size.

To model the effects of space weathering, α is increased by adding to it α_{Fe}, the absorption coefficient of a suspension of Fe particles. If the particles are all much smaller than the wavelength, α_{Fe} can be calculated from the Maxwell-Garnett effective medium theory

$$\alpha_{Fe} = 36\pi z f \rho_h/\lambda\rho_{Fe}$$

where f = mass fraction of SMFe averaged over the whole medium, ρ_h = density of the host silicate medium, ρ_{Fe} = density of Fe particles, λ = wavelength, and

$$z = n_h^3 n_{Fe} k_{Fe}/[(n_{Fe}^2 - k_{Fe}^2 + 2n_h^2)^2 + (2n_{Fe}k_{FE})^2]$$

where n and k are the real and imaginary parts respectively of the refractive index and the subscripts h and Fe refer to the host medium and Fe respectively. Figure 10 shows an example of an application of this model.

8. SPACECRAFT OBSERVATIONS

Several asteroids have been visited by spacecraft. In particular, we have images and a few spectra of the main-belt asteroids 951 Gaspra and 243 Ida obtained by *Galileo* (see *Sullivan et al.,* 2002). In addition, the *NEAR Shoemaker* spacecraft obtained images of 253 Mathilde (*Veverka et al.,*

1999) and then orbited the near-Earth asteroid 433 Eros for one year (see *Cheng,* 2002), mapping the surface and obtaining images (*Veverka et al.,* 2000), 0.8–2.4-μm spectra (*Bell et al.,* 2002), X-ray and γ-ray spectra (*Trombka et al.,* 2000), and laser altimetry (*Zuber et al.,* 2000). In this section we briefly describe some relevant observations for each asteroid, paying special attention to the Eros results because of the high quantity and quality of data obtained on that asteroid.

8.1. 951 Gaspra

Gaspra holds the distinction of being the first main-belt asteroid to be visited by spacecraft. Gaspra is an S-type asteroid, and has been linked with olivine-rich meteorites. *Galileo* flew by Gaspra in 1991, and multispectral images of the surface revealed minor spectral variations associated with morphologically fresh craters on ridges. Specifically, craters on ridges tend to be bluer in color than nearby surrounding terrain. Although the level of color heterogeneity is extremely low (less than 5%), the association of color with craters strengthened the interpretation that these craters excavated relatively fresh subsurface materials (*Clark,* 1993; *Chapman,* 1996).

8.2. 243 Ida

Ida is also an S-type asteroid, and has been linked with pyroxene-rich meteorites such as OCs. On Ida, regolith processes such as crater formation and ejecta emplacement are linked with color variations (*Sullivan et al.,* 1996; *Geissler et al.,* 1996; *Lee et al.,* 1996; *Chapman,* 1996). These color variations were attributed to the exposure of fresh subsurface materials that contrasted with the surrounding surface (*Chapman,* 1996). Color variations on Ida mimic the sense of the color differences due to optical maturity observed on the Moon; however, the magnitude of the variations on Ida is much smaller.

8.3. 253 Mathilde

Mathilde is a C-type asteroid, and has been generally linked with carbonaceous chondrites. *NEAR Shoemaker* images show that Mathilde is uniformly dark, with no fresh exposures (albedo or color variations) near craters or in crater walls (*Veverka et al.,* 1999; *Clark et al.,* 1999). The lack of color and albedo variations on Mathilde's surface argues that surface processes on this dark asteroid do not result in optical alteration. This is not surprising because Mathilde is composed of dark C-rich (opaque) particles, whereas the dominant weathering processes cause the most observable changes to bright transparent particles.

8.4. 433 Eros

Eros is an S-type asteroid that has been linked with L and LL OCs (*McCoy et al.,* 2001). Spectral differences between dark ambient surface and fresher exposures of subsurface materials on Eros mimic the optical alteration expected from space weathering. Psyche, the largest fresh crater on Eros (5.3 km diameter) shows the clearest evidence of space-weathering effects on Eros. Combined imaging and spectrometer observations of Psyche crater reveal distinctive brightness patterns consistent with downslope motion of dark regolith material overlying a substrate of brighter material (Fig. 11) (*Veverka et al.,* 2000; *Murchie et al.,* 2002; *Clark et al.,* 2001). At spatial scales of 620 m, Psyche crater wall materials exhibit albedo contrasts of 30–40% at 0.95 μm, with associated spectral variations at a much lower level of 4–8% (Fig. 12). At spatial scales of 50 m the albedo contrasts are as high as 80% with associ-

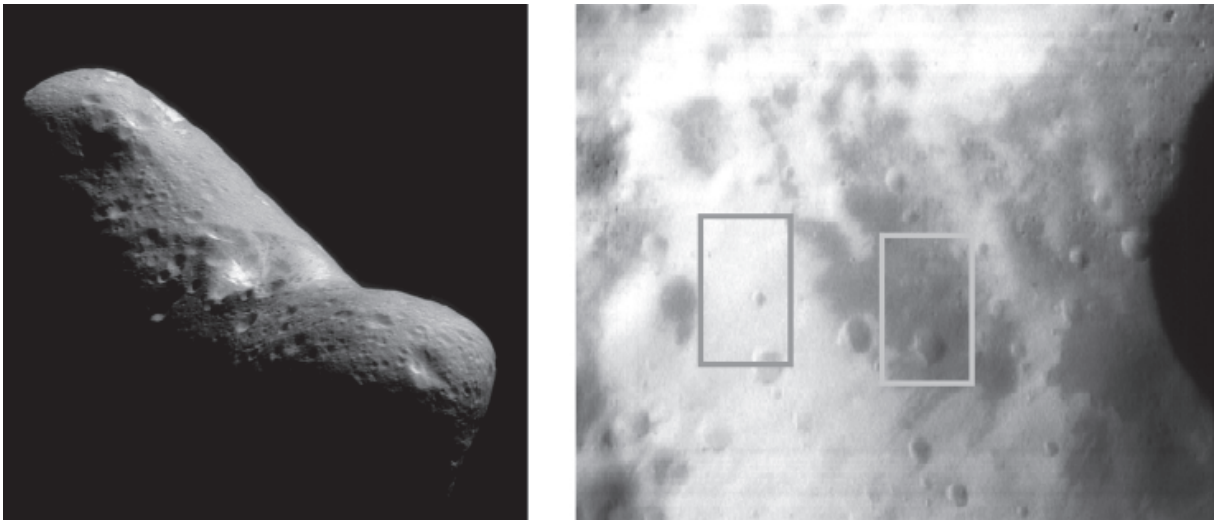

Fig. 11. (left) A NEAR image of Psyche crater on Eros. (right) A zoom image of an area with nearby exposures of bright and dark materials in the walls of Psyche crater (from *Clark et al.,* 2001).

ated spectral contrasts of less than 10% (*Murchie et al.,* 2002). It is unusual to observe such stark albedo contrasts with so little associated color differences. Scattering model and lunar analogy investigations into several possible causes for these albedo and spectral trends reveal that: the contrasts are not consistent with a cause due solely to variations in grain size, olivine, pyroxene, troilite, or lunarlike optical maturation (denoted SMFe) (Fig. 13). A grain size change sufficient to explain the albedo contrasts would result in strong color variations that are not observed. Olivine and pyroxene variations cannot reproduce the albedo contrasts, and would produce strong band-correlated variations that are not observed. Troilite, or dark neutral spectral variations (a proxy for shock-related darkening), would produce bluer color contrasts than are observed, and a simple lunarlike optical maturation effect would produce strong reddening that is not observed. The actual albedo contrasts and associated spectral variation trends are most consistent with a combination of enhanced dark spectrally neutral components and lunarlike optical maturation (*Clark et al.,* 2001). These results suggest that space-weathering processes may explain the differences between bright and dark materials on Eros. However, there are significant spectral differences between Eros' proposed analog meteorites and Eros' freshest exposures of subsurface bright materials. After accounting for all differences in the measurement units of reflectance comparisons, the bright materials on Eros have reflectance values at 0.95 μm consistent with meteorites, but spectral continua that are much redder than meteorites from 1.5 to 2.4 μm. Average Eros surface materials are 30–40% darker than meteorites (*Clark et al.,* 2001).

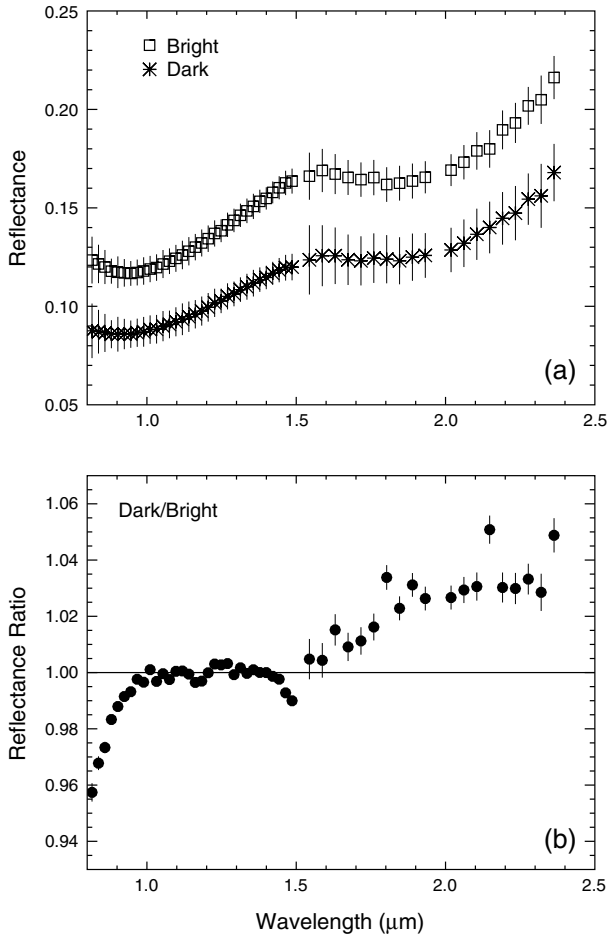

Fig. 12. **(a)** Spectra for dark and bright regions in Psyche crater. **(b)** A normalized spectral ratio of dark/bright materials. This ratio brings out the differences in spectral properties between the dark and bright materials. In general, dark materials tend to be redder from 1.5 to 2.4 μm, and slightly broader in 1-μm band depth from 0.8 to 1.0 μm (from *Clark et al.,* 2001).

The association between color units on Eros is entirely different from associations observed on Gaspra and Ida (*Sullivan et al.,* 1996). On Eros, albedo contrasts are high, color contrasts are low, and bright materials are correlated with steep crater walls (*Thomas et al.,* 2002; *Murchie et al.,* 2002). On Gaspra and Ida albedo contrasts are low, color contrasts are high, and color units appear to be correlated with ejecta emplacement. These geomorphologic associations are important constraints on space weathering of asteroid surfaces. It is possible that Eros does not have bright rimmed craters like Gaspra and Ida have because it is in a different weathering environment in the solar system. Eros is in near-Earth space, whereas Gaspra and Ida are in the main belt. This argues for different rates of the competing processes of surface maturation and impact cratering between near-Earth orbits and the asteroid main belt (for more detail see *Chapman et al.,* 2002).

9. SUMMARY AND FUTURE WORK

9.1. Summary

A description of space weathering on asteroids that is most consistent with the available evidence is as follows. (1) Some lunarlike optical maturation occurs and its strength is dependent on the composition of the target material; however, it is not as effective on asteroids as it is on the Moon. The main process is probably deposition of condensates bearing SMFe on grain surfaces from vaporization of target material by solar wind sputtering and micrometeorite bombardment. (2) Some spectrally neutral darkening occurs and is probably related to the processes of shock, solar wind gas implantation, and contamination by carbonaceous material.

Space-weathering effects on asteroids strongly depend on the composition of the target. Some asteroid types show very little evidence of optical alteration (C types), while other types show strong evidence of optical alteration (S types). These trends indicate that objects composed of dark, relatively opaque components exhibit minimal space-weathering effects while objects composed of bright, relatively transparent components exhibit maximal space-weathering effects. Availability of Fe in target minerals influences the abundance of SMFe. Experiments indicate that olivine is more easily weathered than pyroxene, perhaps explaining

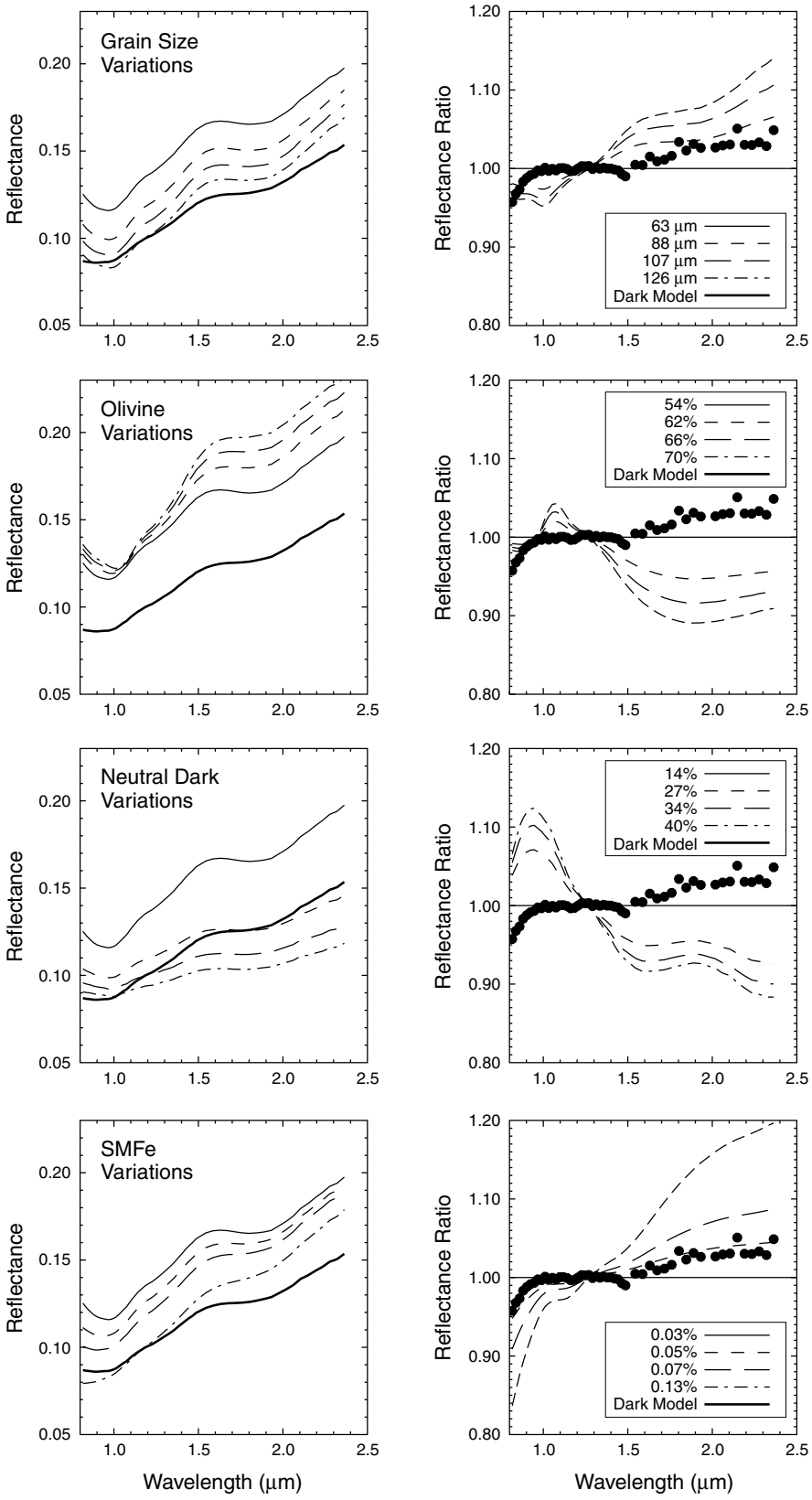

Fig. 13. (left) Each panel shows the bright material spectrum (solid thin line) and the dark material spectrum (solid thick line) compared with variations in the indicated model parameter. (right) In terms of normalized reflectance ratio, each panel compares the observed color trends (solid black dots) to expected color variations given the parameter variations in the left panels. Most parameter variations (except olivine abundance) can produce the observed albedo changes; however, the reflectance ratios indicate that the expected associated color variations are too strong to match the observations. A good explanation for the observed trends would be a combination of the SMFe effects with enhanced neutral dark component (from *Clark et al.,* 2001).

some of the variations in the degree of weathering observed within an asteroid class.

A prediction of the model is that a pristine sample of asteroid regolith in which space weathering has occurred should possess a weak ESR ferromagnetic resonance.

9.2. Remaining Unresolved Issues and Problems

Soil samples from several different asteroid spectral types are needed to verify the compositional dependencies of space-weathering effects. There is no quantitative understanding of the relative rates of the space-weathering processes and their optical effects. In particular, it is not clear why the color and albedo trends due to space weathering on 951 Gaspra and 243 Ida differ from those on 433 Eros.

The values of the complex spectral refractive index of Fe measured by various workers vary greatly (by more than a factor of 2), probably because of surface oxidation effects. Accurate values appropriate to the space environment are badly needed for reliable modeling.

REFERENCES

Adams J. and McCord T. (1971) Optical properties of mineral separates, glass, and anorthositic fragments from Apollo mare samples. *Proc. Lunar Sci. Conf. 2nd,* pp. 2183–2195.

Bell J. F. (1995a) Do ordinary chondrites come from S-class asteroids? Invited talk, AAS Div. for Planetary Sciences, annual meeting, Kona, Hawai'i.

Bell J. F. (1995b) Q-class asteroids and ordinary chondrites (abstract). In *Lunar and Planetary Science XXVI,* pp. 93–94. Lunar and Planetary Institute, Houston.

Bell J. F. (1997) Geochemical space weathering effects on asteroids: Implications for spacecraft instrumentation (abstract). In *Lunar and Planetary Science XXVIII,* pp. 83–84. Lunar and Planetary Institute, Houston.

Bell J. F. (1998) The Vesta asteroid family: Fact or fiction (abstract). In *Lunar and Planetary Science XXIX,* abstract #1851. Lunar and Planetary Institute, Houston (CD-ROM).

Bell J. F. III, Izenberg N. I., Lucey P. G., Clark B. E., Peterson C., Gaffey M. J., Joseph J., Carcich B., Harch A., Bell M. E., Warren J., Martin P. D., McFadden L. A., Wellnitz D., Murchie S., Winter M., Veverka J., Thomas P., Robinson M. S., Malin M., and Cheng A. (2002) Near-IR reflectance spectroscopy of 433 Eros from the NIS instrument on the NEAR mission. 1. Low phase angle observations. *Icarus, 155,* 119–144.

Bell P. M., Mao H. K., and Weeks R. A. (1976) Optical spectra and electron paramagnetic resonance of lunar and synthetic glasses: A study of the effects of controlled atmosphere, composition, and temperature. *Proc. Lunar Sci. Conf. 7th,* pp. 2543–2559.

Binzel R. P. and Xu S. (1993) Chips off asteroid 4 Vesta: Evidence for the parent body of basaltic achondrite meteorites. *Science, 260,* 186–191.

Binzel R. P., Bus S. J., Burbine T. H., and Sunshine J. M. (1996) Spectral properties of near-Earth asteroids: Evidence for sources of ordinary chondrite meteorites. *Science, 273,* 946–948.

Bobrovnikoff N. T. (1929) The spectra of minor planets. *Lick Observatory Bull., 14 (407),* 18–27.

Britt D. and Pieters C. M. (1994) Darkening in black and gas-rich ordinary chondrite meteorites: The spectral effects of opaque morphology and distribution. *Geochim. Cosmochim. Acta., 58,* 3905–3919.

Britt D., Tholen D. J., Bell J. F., and Pieters C. M. (1992) Comparison of asteroid and meteorite spectra: Classification by principal components analysis. *Icarus, 99,* 153–166.

Burbine T. (1991) Principal component analysis of asteroid and meteorite spectra from 0.3 to 2.5 microns. Master's thesis, Univ. of Pittsburgh, Pittsburgh, Pennsylvania.

Carr M., Kirk R., McEwan A., Veverka J., Thomas P., Head J., and Murchie S. (1994) The geology of Gaspra. *Icarus, 107,* 61–71.

Cassidy W. and Hapke B. (1975) Effects of darkening processes on surfaces of airless bodies. *Icarus, 25,* 371–383.

Chapman C. (1995) Do ordinary chondrites come from S-class asteroids? Invited talk, AAS Div. for Planetary Sciences, annual meeting, Kona, Hawai'i.

Chapman C. (1996) S-type asteroids, ordinary chondrites and space weathering: The evidence from Galileo's fly-bys of Gaspra and Ida. *Meteoritics & Planet. Sci., 31,* 699–725.

Chapman C. and Salisbury J. (1973) Comparisons of meteorite and asteroid spectral reflectivities. *Icarus, 19,* 507–522.

Chapman C. R., Merline W. J., Thomas P. C., Joseph J., Cheng A. F., and Izenberg N. (2002) Impact history of Eros: Craters and boulders. *Icarus, 155,* 104–118.

Cheng A. F. (2002) Near Earth Asteroid Rendezvous: Mission summary. In *Asteroids III* (W. F. Bottke Jr. et al., eds.), this volume. Univ. of Arizona, Tucson.

Clark B.E. (1993) Spectral reflectance studies and optical surface alteration in the search for links between meteorites and asteroids. Ph.D. dissertation, Univ. of Hawai'i.

Clark B. E. and Johnson R. E. (1996) Interplanetary weathering: Surface erosion in outer space. *Eos Trans. AGU, 77,* 141–145.

Clark B. E., Fanale F., and Salisbury J. (1992) Meteorite-asteroid spectral comparison: The effects of comminution, melting and recrystallization. *Icarus, 97,* 288–297.

Clark B. E., Veverka J., Helfenstein P., Thomas P., Bell J. F. III, Harch A., Robinson M., Murchie S., McFadden L., and Chapman C. (1999) NEAR photometry of asteroid 253 Mathilde. *Icarus, 140,* 53–65.

Clark B. E., Lucey P., Helfenstein P., Bell J. F. III, Peterson C., Veverka J., McConnochie T., Robinson M., Bussey B., Murchie S., Izenberg N., and Chapman C. (2001) Space weathering on Eros: Constraints from albedo and spectral measurements of Psyche crater. *Meteoritics & Planet. Sci., 36,* 1617–1637.

Clark B. E., Helfenstein P., Bell J. F. III, Peterson C., Veverka J., Izenberg N. I., Domingue D., Wellnitz D., and McFadden L. (2002) NEAR infrared spectrometer photometry of asteroid 433 Eros. *Icarus, 155,* 189–204.

Clark R. N. and Roush T. L. (1984) Reflectance spectroscopy: Quantitative analysis techniques for remote sensing applications. *J. Geophys. Res., 89,* 6329–6340.

Cloutis E. and Gaffey M. (1993) Lunar regolith analogues: Spectral reflectance properties of compositional variations. *Icarus, 102,* 203–224.

Conel J. and Nash D. (1970) Spectral reflectance and albedo of Apollo 11 lunar samples: Effects of irradiation and vitrification and comparison with telescopic observations. *Proc. Apollo 11 Lunar Sci. Conf.,* pp. 2013–2024.

Dollfus A., Wolff M., Geake J., Lupishko D., and Dougherty L. (1989) Photopolarimetry of asteroids. In *Asteroids II* (R. P. Binzel et al., eds.), pp. 594–616. Univ. of Arizona, Tucson.

Dukes C. A., Baragiola R. A., and McFadden L. A. (1999) Surface modification of olivine by H^+ and He^+ bombardment. *J.*

Geophys. Res., 104, 1865–1872.
Fanale F., Clark B. E., and Bell J. F. (1992) A spectral analysis of ordinary chondrites, S-type asteroids and their component minerals: Genetic implications. *J. Geophys. Res., 97,* 20863–20874.
Gaffey M. J. (1976) Spectral reflectance characteristics of the meteorite classes. *J. Geophys. Res., 81,* 905–920.
Gaffey M. J., Bell J. F., Brown R. H., Burbine T. H., Piatek J. L., Reed K. L., and Chaky D. A. (1993) Mineralogical variations within the S-type asteroid class. *Icarus, 106,* 573–602.
Geissler P., Petit J. M., Durda D., Greenberg R., Bottke W., Nolan M., and Moore J. (1996) Erosion and ejecta reaccretion on 243 Ida and its moon. *Icarus, 120,* 140–157.
Gold T. (1955) The lunar surface. *Mon. Not. R. Astron. Soc., 115,* 585–604.
Hapke B. (1966) Optical properties of the moon's surface. In *The Nature of the Lunar Surface* (W. Hess et al., eds.), pp. 141–154. Johns Hopkins, Baltimore.
Hapke B. (1968) The composition of the lunar surface inferred from optical properties. *Science, 159,* 76–79.
Hapke B. (1973) Darkening of silicate rocks by solar wind sputtering. *Moon, 7,* 342–355.
Hapke B. (1993) *Theory of Reflectance and Emittance Spectroscopy*. Cambridge Univ., New York.
Hapke B. (2000) How to turn OC's into S's: Space weathering in the asteroid belt (abstract). In *Lunar and Planetary Science XXXI,* abstract #1087. Lunar and Planetary Institute, Houston (CD-ROM).
Hapke B. (2001) Space weathering from Mercury to the asteroid belt. *J. Geophys. Res., 106,* 10039–10073.
Hapke B., Cassidy W., and Wells E. (1975) Effects of vapor-phase deposition processes on the optical, chemical and magnetic properties of the lunar regolith. *Moon, 13,* 339–354.
Heiken G. H., Vaniman D. T., and French B. M., eds. (1991) *Lunar Sourcebook: A User's Guide to the Moon.* Cambridge Univ., New York. 736 pp.
Heymann D. (1967) On the origin of hypersthene chondrites: Ages and shock effects of black chondrites. *Icarus, 6,* 189–221.
Hiroi T. and Sasaki S. (2002) Importance of space weathering simulation products in compositional modeling of asteroids: 349 Dembowska and 446 Aeternitas as examples. *Meteoritics & Planet. Sci., 36,* 1587–1596.
Hiroi T., Pieters C., and Takeda H. (1994) Grain size of the surface regolith of asteroid 4 Vesta estimated from its reflectance spectrum in comparison with HED meteorites. *Meteoritics, 29,* 394–396.
Hiroi T., Binzel R., Sunshine J., Pieters C., and Takeda H. (1995) Grain sizes and mineral compositions of surface regoliths of Vesta-like asteroids. *Icarus, 115,* 374–386.
Hiroi T., Pieters C. M., Vilas F., Sasaki S., Hamabe Y., and Kurahashi E. (2000) Possible space weathering of Vesta and Vestoids evident in their reflectance spectra (abstract). *Eos Trans. AGU, 81,* WP1-1-102.
Hörz F. and Cintala M. (1997) Impact experiments related to the evolution of planetary regoliths. *Meteoritics & Planet. Sci., 32,* 179–209.
Housen K. R. and Wilkening L. L. (1982) Regoliths on small bodies in the solar system. *Annu. Rev. Earth Planet. Sci., 10,* 355–376.
Johnson P. and Christy R. (1974) Optical constants of transition metals: Ti, V, Cr, Mn, Fe, Co, Ni and Pd. *Phys. Rev., B9,* 5056–5070.
Keil K. (1982) Composition and origin of chondritic breccias. In *Workshop on Lunar Breccias and Soils and Their Meteoritic Analogs* (G. J. Taylor and L. L. Wilkening, eds.), pp. 65–83. LPI Tech. Rpt. 82-02, Lunar and Planetary Institute, Houston.
Keil K., Bell J. F., and Britt D. T. (1992) Reflection spectra of shocked ordinary chondrites and relations to C-type and K-type asteroids. *Icarus, 98,* 43–53.
Keller L. P. and McKay D. S. (1993) Discovery of vapor deposits in the lunar regolith. *Science, 261,* 1305–1307.
Keller L. P. and McKay D. S. (1997) The nature and origin of rims on lunar soil grains. *Geochim. Cosmochim. Acta., 61,* 2331–2341.
Keller L. P., Wentworth S. J., and McKay D. S. (1998) Surface-correlated nanophase iron metal in lunar soils: Petrography and space weathering effects. In *Workshop on New Views of the Moon: Integrated Remotely Sensed, Geophysical, and Sample Datasets,* pp. 44–45. LPI Contribution No. 958, Lunar and Planetary Institute, Houston.
Keller L. P., Wentworth S. J., McKay D. S., Taylor L. A., Pieters C. M., and Morris R. V. (1999) Space weathering in the fine size fractions of lunar soils: Mare/highland differences. In *Workshop on New Views of the Moon II: Understanding the Moon Through the Integration of Diverse Datasets,* pp. 32–33. LPI Contribution No. 980, Lunar and Planetary Institute, Houston.
KenKnight C., Rosenberg D., and Wehner G. (1967) Parameters of the optical properties of the lunar surface powder in relation to solar wind bombardment. *J. Geophys. Res., 72,* 3105–3130.
Lee P., Veverka J., Thomas P., Helfenstein P., Belton M. J. S., Chapman C., Greenberg R., Pappalardo R., Sullivan R., and Head J. (1996) Ejecta blocks on 243 Ida and on other asteroids. *Icarus, 120,* 87–105.
Lucey P. G., Taylor G., and Malaret E. (1995) Abundance and distribution of iron on the Moon. *Science, 268,* 1150–1153.
Lucey P. G., Blewett D. T., Taylor G. J., and Hawke B. R. (2000) Imaging of lunar surface maturity. *J. Geophys. Res., 105,* 20377–20386.
Matson D., Johnson T., and Veeder G. (1977) Soil maturity and planetary regoliths: The Moon, Mercury and the asteroids. *Proc. Lunar Sci. Conf. 8th,* pp. 1001–1011.
McCord T. B., Adams J., and Johnson T. (1970) Asteroid Vesta: Spectral reflectivity and compositional implications. *Science, 168,* 1445–1447.
McCord T. B., Clark R. N., Hawke B. R., McFadden L. A., Owensby P. D., Pieters C. M., and Adams J. B. (1981) Moon: Near infrared spectral reflectance, a first good look. *J. Geophys. Res., 86,* 10883–10892.
McCoy T. J., Burbine T. H., McFadden L. A., Starr R. D., Gaffey M. J., Nittler L. R., Evans L. G., Izenberg N., Lucey P., Trombka J., Bell J. F. III, Clark B. E., Clark P. E., Squyres S. W., Chapman C. R., Boynton W. V., and Veverka J. (2001) The composition of 433 Eros: A mineralogical-chemical synthesis. *Meteoritics & Planet. Sci., 36,* 1661–1672.
McKay D. S., Fruland R. M., and Heiken G. H. (1974) Grain size and evolution of lunar soils. *Proc. Lunar Sci. Conf. 5th,* pp. 887–906.
McKay D., Swindle T., and Greenberg R. (1989) Asteroidal regoliths: What we do not know. In *Asteroids II* (R. P. Binzel et al., eds.), pp. 617–642. Univ. of Arizona, Tucson.
Moroz L., Fisenko A., Semjonova L., Pieters C., and Korotaeva N. (1996) Optical effects of regolith processes on S-asteroids as simulated by laser shots on ordinary chondrite and other mafic materials. *Icarus, 122,* 366–382.
Morris R. V. (1976) Surface exposure indices of lunar soils: A

comparative FMR study. *Proc. Lunar Sci. Conf. 7th,* pp. 315–335.

Morris R. V. (1977) Origin and evolution of the grain-size dependence of the concentration of fine-grained metal in lunar soils: The maturation of lunar soils to a steady-state stage. *Proc. Lunar Sci. Conf. 8th,* pp. 3719–3747.

Morris R. V. (1978) The surface exposure (maturity) of lunar soils: Some concepts and I_s/FeO compilation. *Proc. Lunar Planet. Sci. Conf. 9th,* pp. 2287–2297.

Morris R. V. (1980) Origins and size distribution of metallic iron particles in the lunar regolith. *Proc. Lunar Planet. Sci. Conf. 11th,* pp. 1697–1712.

Murchie S., Robinson M., Clark B., Li H., Thomas P., Joseph J., Bussey B., Domingue D., Veverka J., Izenberg N., and Chapman C. (2002) Color variations on Eros from NEAR multispectral imaging. *Icarus, 155,* 145–168.

Noble S. K., Pieters C. M., Taylor L. A., Morris R. V., Allen C. C., McKay D. S., and Keller L. P. (2001) Optical properties of the finest fraction of lunar soils: Implications for space weathering environments. *Meteoritics & Planet. Sci., 36,* 31–42.

Pieters C. M. (1983) Strength of mineral absorption features in the transmitted component of near-infrared light: First results from RELAB. *J. Geophys. Res., 88,* 9534–9544.

Pieters C. M. (1986) Composition of the lunar highland crust from near-infrared spectroscopy. *Rev. Geophys. Space Phys., 24,* 557–578.

Pieters C. M. and Binzel R. P. (1994) Young Vesta (regolith)? (abstract). In *Lunar and Planetary Science XXV,* pp. 1083–1084. Lunar and Planetary Institute, Houston.

Pieters C. M. and McFadden L. (1994) Meteorite and asteroid reflectance spectroscopy: Clues to early solar system processes. *Annu. Rev. Earth Planet. Sci., 22,* 457–497.

Pieters C. M., Fischer E., Rode O., and Basu A. (1993) Optical effects of space weathering: The role of the finest fraction. *J. Geophys. Res., 98,* 20817–20824.

Pieters C. M., Taylor L., Noble S., Keller L., Hapke B., Morris R., Allen C., McKay D., and Wentworth S. (2000) Space weathering on airless bodies: Resolving a mystery with lunar samples. *Meteoritics & Planet. Sci., 35,* 1101–1107.

Rosenberg D. and Wehner G. (1964) Darkening of powdered basalt by simulated solar wind. *J. Geophys. Res., 69,* 3307–3308.

Rubin A. E., Scott E. R. D., and Keil K. (1997) Shock metamorphism of enstatite chondrites. *Geochim. Cosmochim. Acta, 61,* 847–858.

Sasaki S., Nakamura K., Hamabe Y., Kurahashi E., and Hiroi T. (2001) Production of iron nanoparticles by laser irradiation in a simulation of lunar-like space weathering. *Nature, 410,* 555–557.

Shkuratov Y., Kreslavsky M., Ovcharenko A., Stankevich D., Zubko E., Pieters C., and Arnold G. (1999) Opposition effect from Clementine data and mechanisms of backscatter. *Icarus, 141,* 132–155.

Sullivan R., Greeley R., Pappalardo R., Asphaug E., Moore J., Morrison D., Belton M. J. S., Carr M., Chapman C., Geissler P., Greenberg R., Granahan J., Head J., Kirk R., McEwan A., Lee P., Thomas P., and Veverka J. (1996) Geology of 243 Ida. *Icarus, 120,* 119–139.

Sullivan R. J., Thomas P. C., Murchie S. L., and Robinson M. S. (2002) Asteroid geology from *Galileo* and *NEAR Shoemaker* data. In *Asteroids III* (W. F. Bottke Jr. et al., eds.), this volume. Univ. of Arizona, Tucson.

Taylor L. A., Pieters C. M., Morris R. V., Keller L., and McKay D. (2001a) Lunar mare soils: Space weathering and the major effects of surface-correlated nanophase Fe. *J. Geophys. Res., 106,* 27985–28000.

Taylor L. A., Cahill J. T., Patchen A., Pieters C. M., Morris R. V., Keller L., and McKay D. (2001b) Mineralogical and chemical characterization of lunar highland regolith: Lessons learned from mare soils (abstract). In *Lunar and Planetary Science XXXII,* abstract #2196. Lunar and Planetary Institute, Houston (CD-ROM).

Tedesco E. F., Matson D., and Veeder G. (1989) Classification of IRAS asteroids. In *Asteroids II* (R. P. Binzel et al., eds.), pp. 290–297. Univ. of Arizona, Tucson.

Thomas P. C., Joseph J., Carcich B., Veverka J., Clark B. E., Bell J. F. III, Byrd A. W., Chomko R., Robinson M., Murchie S., Prockter L., Cheng A., Izenberg N., Malin M., Chapman C., McFadden L. A., Kirk R., Gaffey M., and Lucey P. G. (2002) Eros: Shape, topography, and slope processes. *Icarus, 155,* 18–37.

Trombka J., Squyres S., Bruckner J., Boynton W., Reedy R., McCoy T., Gorenstein P., Evans L., Arnold J., Starr R., Nittler L., Murphy M., Mikheeva I., McNutt R., McClanahan T., McCartney E., Goldsten J., Gold R., Floyd S., Clark P., Burbine T., Bhangoo J., Bailey S., and Pataev M. (2000) The elemental composition of asteroid 433 Eros: Results of the NEAR Shoemaker X-ray spectrometer. *Science, 289,* 2101–2105.

Veverka J., Thomas P., Harch A., Clark B. E., Bell J. F. III, Carcich B., Joseph J., Murchie S., Izenberg N., Chapman C., Merline W., Malin M., McFadden L., and Robinson M. (1999) NEAR encounter with asteroid 253 Mathilde: Overview. *Icarus, 140,* 3–16.

Veverka J., Robinson M., Thomas P., Murchie S., Bell J. F. III, Izenberg N., Chapman C., Harch A., Bell M., Carcich B., Cheng A., Clark B. E., Domingue D., Dunham D., Farquhar R., Gaffey M., Hawkins E., Joseph J., Kirk R., Li H., Lucey P., Malin M., Martin P., McFadden L., Merline W., Miller J., Owen W., Peterson C., Proktor L., Warren J., Wellnitz D., Williams B., and Yeomans D. (2000) NEAR at Eros: Imaging and spectral results. *Science, 289,* 2088–2097.

Veverka J., Thomas P. C., Robinson M., Murchie S., Chapman C., Bell M., Harch A., Merline W. J., Bell J. F. III, Bussey B., Carcich B., Cheng A., Clark B. E., Domingue D., Dunham D., Farquhar R., Gaffey M. J., Hawkins E., Izenberg N., Joseph J., Kirk R., Li H., Lucey P., Malin M., McFadden L., Miller J. K., Owen W., Peterson C., Procktor L., Warren J., Wellnitz D., Williams B., and Yeomans D. K. (2001) Imaging of small-scale features on 433 Eros from NEAR: Evidence for a complex regolith. *Science, 292,* 484–488.

Wells E. and Hapke B. (1977) Lunar soil: Iron and titanium bands in the glass fraction. *Science, 195,* 977–979.

Yamada M., Sasaki S., Nagahara H., Fujiwara A., Hasegawa S., Yano H., Hiroi T., Ohashi H., and Otake H. (1999) Simulation of space weathering of planet-forming materials: Nanosecond pulse laser irradiation and proton implantation on olivine and pyroxene samples. *Earth Planets Space, 51,* 1255–1265.

Zuber M., Smith D., Cheng A., Garvin J., Aharonson O., Cole T., Dunn P., Guo Y., Lemoine F., Neumann G., Rowlands D., and Torrence M. (2000) The shape of 433 Eros from the NEAR Shoemaker Laser Rangefinder. *Science, 289,* 2097–2102.